Wave-induced cross-shore distribution of different densities, shapes, and sizes of plastic debris in coastal environments: a laboratory experiment

Paula Núñez[a,*], Alessandro Romano[b,a], Javier García-Alba[a], Giovanni Besio[c], Raúl Medina[a]

[a]*IHCantabria - Instituto de Hidráulica Ambiental de la Universidad de Cantabria, Santander, Spain*
[b]*Roma Tre University, Engineering Department, Via Vito Volterra, 62 - 00146, Rome, Italy*
[c]*DICCA, University of Genoa, 1 Via Montallegro, I-16145 Genoa, Italy*

Abstract

Plastic debris is a significant threat to marine and coastal ecosystems. Previous research found that waves, wind, as well as density, size, and shape of microplastics, drive their transport and dispersion. In this paper, a set of laboratory experiments on the effect of waves and wave-induced currents on the input rate and cross-shore transport and dispersion of different types of plastic debris, including the macro and mesosizes, in addition to microplastics is presented. 15 plastic-debris types characterized by different sizes, shapes, and densities, including facemasks, were analyzed under regular and irregular wave conditions. The results show that input and transport rates of plastics depend on their terminal velocities and wave steepness. Plastics with higher settling velocities under less-steep wave conditions are likely to escape coastal entrapment and end up in the breaking zone. However, plastics with greater buoyancy rates under steeper waves show a predominant accumulation closer to the shoreline.

Keywords: Plastic debris, Pollution, Waves, Nearshore zone, Transport

*Corresponding author
Email address: nunezp@unican.es (Paula Núñez)

mechanisms, Terminal velocity

1. Introduction

Marine litter is one of the main current threats to marine and coastal ecosystems (Derraik, 2002; Jambeck et al., 2015; Van Sebille et al., 2020). Plastic material represents more than 80% of the total amount of marine litter that reaches the ocean (Derraik, 2002; Barnes et al., 2009; Villarrubia-Gómez et al., 2018), affecting habitats, ecosystems, species, human health, and economic activities such as fishing, tourism, and navigation (Hardesty et al., 2017). A widely accepted classification of plastic debris proposed by Crawford and Quinn (2017) is based on their size, namely: macro (> 25 mm), meso (5−25 mm), and microplastics (< 5 mm). Macro and mesoplastics represent a significant risk for the entrapment of marine fauna (Derraik, 2002), while microplastics can be ingested by marine mammals, fish, birds, and planktonic organisms (Galloway et al., 2017), can provide a favorable substrate for the development of undesirable microorganisms (e.g., fish pathogens) (Barnes et al., 2009), and also play an important role in the transport of toxic chemicals (Wang et al., 2017; Gallo et al., 2018). The growing concern about the problem of marine litter is evident in international environmental agendas, such as the EU Marine Strategy Framework Directive (MSFD, Galgani et al., 2013).

Several studies investigated the behavior of drifting macro and mesoplastics in large-scale ocean circulation (on the global and regional scales) using numerical approaches (e.g., Law et al. (2010); Lebreton et al. (2012); Maximenko et al. (2012); Van Sebille et al. (2012) on the global scale, or Kako et al. (2011, 2014); Zambianchi et al. (2014, 2017) on the regional scale). Other studies focused on analyzing the dispersion of plastic debris in coastal and estuarine environments (local scale). Most of these local-scale studies were based on the analysis of field data (e.g. Mazarrasa et al., 2019; van Emmerik et al., 2022) and a few evaluated, through numerical approaches, the role that tidal asymmetry plays in the dispersion processes (Núñez et al., 2019, 2020, 2021).

In the last decade, research addressed the study of microplastics and provided some insights about plastic-debris dispersion in open oceans and coastal areas, highlighting the relevant role played by waves (Law et al., 2010; Heo et al., 2013; Isobe et al., 2014; Critchell and Lambrechts, 2016; Stocchino et al., 2019; Cunningham et al., 2022). Recent experimental studies assessed the role of wind and regular waves in the inertial dynamics of different sizes, shapes, and densities of plastic debris in small-scale wave flumes. Forsberg et al. (2020) and Kerpen et al. (2020) found that the high-density microplastics behave like natural sand and show dominant accumulation in the breaking zone, while light particles show variable accumulation along the coastal profile depending on wind and wave characteristics, and particle shape. Alsina et al. (2020) addressed the study of relatively larger spherical particles (mesoplastics) in intermediate water depth. Authors found that non-buoyant particles move near the bed with magnitudes of velocity lower than the motion of particles floating at the free surface. De Leo et al. (2021) found that the net settling velocity of microplastics depends not only on the particle features, but also on the wave characteristics. The net settling velocity of spherical microplastics in a fluid subjected to wave action is significantly higher than the settling velocity in still water, and this effect is more evident for larger particles. The aforementioned laboratory studies provided a preliminary understanding of the behavior of some specific types of meso and microplastics in coastal areas under different conditions of wind and regular waves. However, as the Authors themselves underline, further studies are needed due to the complexity of the problem at hand.

This study aims to provide an aggregate description of the cross-shore distribution patterns of very different types of plastic debris in the near-shore zone using physical modeling. A new set of two-dimensional (2DV) vertical laboratory experiments was performed to increase the emerging knowledge of the literature on this topic, including the following points of novelty: I) the behavior of several types of plastic debris of different densities, shapes, and sizes, including macro, meso, and micro-sizes, are assessed; II) the cross-shore transport and dispersion of both plastic debris present in the water and those located on the shoreline were assessed. The analysis of this last condition provides information about the input rates from land to sea, an important aspect considering that 80% of the plastic debris in the ocean comes from land-based sources (Lee et al., 2013; Rech et al., 2014; Galgani et al., 2015). III) Finally, not only regular waves but also irregular wave conditions were evaluated as transport drivers to give a novel insight into the effect of randomness. The results complete and expand the database existing in the literature on the cross-shore distribution of plastic debris due to wind and waves. The experimental extended database is significant to validate predictive numerical tools for the transport of plastic debris as has been done for oil spill models, since experimental, field, and satellite data are useful for this purpose (Abascal et al., 2007, 2009b,a; Cardenas et al., 2015; Gurumoorthi et al., 2021; Naz et al., 2021).

2. Materials and methods

2.1. Experimental setup

The experiments were performed in the 2DV wave flume of the University of Cantabria (Spain), which is 20.0 *m* long, 0.6 *m* wide, and 0.75 *m* high (Fig. 1a and f). The wave flume is equipped with a hydraulically driven piston-type paddle with a stroke length of approximately 1.0 m. The standard generation software AWASYS is used, which can generate both regular and irregular waves with an active wave absorption system. The experimental setup is represented by a fixed bathymetry made up of a horizontal bottom and a straight profile that resembles a dissipative beach. The part with a constant depth of 0.45 m starts at the wave maker and is 8.6 m long. A straight beach with a fixed methacrylate bottom and a 1:20 slope extends to the end of the flume (see Fig. 1f).

Two regular wave (W1 and W2) and an irregular wave (W3) conditions were reproduced at the wave maker position. The target signal for the regular wave conditions is defined by a wave height (H) and a wave period (T). Thus, H 0.18 m and T 1.5 s are defined for W1, and H 0.1 m and T 2.0 s for W2. The irregular sea state W3 is described by a significant spectral wave height (H_{m0}) of 0.1 m, a peak wave period (T_p) of 1.5 s, a TMA (Texel-Marsen-Arsloe) spectrum for shallow water with γ 3.3 and 2^{nd} order subharmonics and superharmonics (Monismith, 2020), and approximately 1000 waves. The two regular sea states W1 and W2 were selected by varying the parameter HgT^2 to explore different transport conditions, while looking for wave breaking in spilling at the beginning and end of the beach profile, respectively (Stocchino et al., 2019). An intermediate energetic condition between W1 and W2 was selected for the irregular sea state W3 to give a first insight into the effect of the randomness (Romano et al., 2015). It is worth noting that no specific scale factor was selected (λ 1) in this laboratory experiment and, therefore, the behavior of plastic debris under small waves was assessed.

The free surface elevation time series was recorded with 10 wave gauges (WG) distributed along the wave flume as shown in Fig. 1f and a sampling frequency of 50

Hz. Wave-induced currents were investigated at different depths, before and after the break positions, using 8 Acoustic Doppler Velocimeters (ADVs) at a sampling rate of 50 Hz (Fig. 1f). ADV_{01-03} were located near the following depths: 39, 33, and 20 *cm*, respectively, where the total depth is 45 *cm*; ADV_{04-06} at 25, 21, and 14 *cm* (total depth of 30 *cm* in this location due to the beach profile); ADV_{07} at 5 *cm* (total depth of 20 *c*m); ADV_{08} at 5 *cm* (total depth of 12 *cm*), respectively. This placement of ADVs responds to the need to describe each of the hydrodynamics in an aggregated way and as completely as possible to analyze the behavior of a wide range of plastic debris based on their buoyancy rates. To track the position of the plastic debris, 8 High-Definition video cameras (4 MP Fixed Bullet Network Cameras, HIKVISION) with a 4 *mm* lens, a resolution of 2560 x 1440 pixels, and a frame rate of 20 fps were used. Four cameras were placed in the zenithal position to cover the entire length of the wave flume. The remaining four cameras were placed in a lateral position to qualitatively describe the 2DV behavior in the beach profile (Fig. 1f).

2.2. Plastic materials

The plastic materials under study were selected among the plastic materials with a significant presence in the marine environment, namely: polyethylene (PE: 900–990 kgm^3), polypropylene (PP: 850–950 kgm^3), polystyrene (950–1100 kgm^3), and polyvinylchloride (PVC: 1100–1580 kgm^3) (Zhang, 2017; Mazarrasa et al., 2019). Moreover, face masks (380–450 kgm^3; Bandi, 2020) were included because of their widespread use in recent years due to the global COVID-19 pandemic (De-la Torre and Aragaw, 2021). Different shapes and sizes of these materials were considered, since these characteristics together with the specific density define their buoyancy and therefore their position in the water column, causing them to be affected by different transport mechanisms (Filella, 2015; Chubarenko and Stepanova, 2017; Zhang, 2017).

A total of 15 types of plastic debris (hereinafter P_i, i = 1,...,15) were evaluated. Fig. 2 and Tab. 1 gather the main characteristics of these materials, namely: specific density (ρ_P); shape, represented by the Corey shape factor (csf); and size, defined by the nominal diameter (D_n).

Test materials, listed from the highest to the lowest density, are: P1 to P6, 2D flexible PVC elements (1340 kgm^3); P8, cylindrical elastane polyester items (part of the face masks, 1020 kgm^3); P9 to P12, 2D low-density polyethylene elements (LDPE; 910 kgm^3); P14 and P15, polypropylene hollow cylindrical elements (PP; 900 kgm^3); P7 and P13, face masks and their fragments, respectively (380 kgm^3). The plastic densities are obtained from manufacturer information when available, reference and literature values (Zhang, 2017; Bandi, 2020).

The Corey shape factor is a non-dimensional parameter which relates the dimensions of plastic debris ($csf \quad c\sqrt{a \cdot b}$, where a, b, and c are the longest, intermediate, and shortest axes) providing information about its shape. csf is close to 0 for 2D shapes and 1 for perfect spheres (Corey, 1949). csf varies between 0.0004 for P10 and 0.77 for P15.

The nominal diameter, defined according to the shape and dimensions of plastic debris (Francalanci et al., 2021), varies between 1.2 mm for P12 and 28.4 mm for P7, covering the entire range of macro, meso, and microplastics. Test-material sizes are obtained from measurements of at least 20 particles of each type. As far as measurements are concerned, the size of plastic debris was measured with a caliper of 0.05 mm resolution and graduated scales of 1 mm resolution. Material thicknesses are always provided by the manufacturer.

It is worth noting that the behaviors of these plastic materials were assessed in freshwater whose density (ρ_w) is about 1000 kgm^3 at a temperature of the water of 14°C. Fig. 1b-d shows some examples of the test plastic materials.

2.2.1. Terminal velocities

The terminal settling and rising velocities ($\omega_{s,r}$, where the subscripts s and r refer to settling and rising, respectively) were inferred for individual items, representative of the different plastic-debris types, and 70 *cm* of still water in a section of the wave flume close to the wave-generation area. Before these estimates, plastic materials were kept submerged in fresh water to avoid possible changes in buoyancy that could be caused by the presence of air bubbles. As initial conditions for non-buoyant items, 5 *cm* below the water surface was chosen to avoid surface tension effects, while buoyant materials were deposited at the bottom of the wave flume. Then, the uppest 10 *cm* and the lowest 10 *cm* of the water column were discarded for non-buoyant and buoyant items, respectively, and the time it takes for plastic debris to travel 50 *cm* of water was recorded. Discarding 10 cm is considered to be enough to reach the terminal velocities considering that movements are mainly in a direction perpendicular to the maximum projected area, a condition which is likely to occur (Stringham et al., 1969; Komar and Reimers, 1978; Middleton and Southard, 1978), and that the thickness of the tested materials is smaller than 2 mm, i.e., 2 orders of magnitude smaller than the 10 cm above mentioned.

In this study, a minimum of five repetitions was performed to estimate the terminal velocity of each plastic material and the average value is provided. It is worth noticing that providing exact measurements of terminal velocities is not an objective of this study, rather terminal velocities are used for relative comparison (i.e., considering the relative degree of buoyancy of different plastic debris) to interpret the physics of the plastic debris under hydrodynamics forcing (i.e., waves and wave-induced currents). Therefore, the Francalanci's formulae (Francalanci et al., 2021), valid for a wide range of plastic shapes (3D, 2D, and 1D) and compositions in quiescent fluids, were used as a cross-check of the reliability of these estimates, although these formulae have not been tested for large and flexible particles.

2.3. Experimental methodology

Each plastic material was tested individually in the wave flume in order to assess its cross-shore transport, distribution, and input rates. The experiments were performed in two steps. In the first step, wave conditions were run without the plastic debris, aiming at calibrating the sea states and measuring the hydrodynamic characteristics. Then, all the instruments were removed from the flume (keeping only the cameras) to avoid singularities that can affect the hydrodynamic behavior of plastic debris and the experiments with plastic debris were carried out.

Regarding the initial conditions for the release of plastic debris, each type was introduced in the wave flume considering two hypotheses. On the one hand, plastic items were randomly released on the run-up zone (IC_{shore}) to take into account plastic debris coming from the beach (Fig. 1c). This initial condition is used to analyze the input rate of plastic debris from land to sea. Two initial arrangements, or degrees of packing, were tested for elongated plastic materials P4, P5, and P6 under this initial condition. These are qualitatively defined as "high" (high degree of overlapping and braiding between items, from P4 to P6) and “low” (dispersed and extended items without connections between them, from P4E to P6E). On the other hand, plastic debris was distributed uniformly throughout the wave flume ($IC_{distributed}$) to analyze the dispersion of plastic debris already present in the marine environment.

Each of these experiments did not last more than 18 minutes, which is the duration of the W3 sea state. The stationary state of plastic debris, i.e., when no significant movement of plastic debris was observed, for W1 and W2 was reached within the first 8 minutes and depended on the type of plastic debris analyzed. At the end of each experiment, immediately after stopping the wave maker, the flume was manually divided into five areas (offshore, shoaling, breaking, surf, and beach) following the Forsberg et al. (2020)’s method. Thus, the plastic material trapped in each area was recovered, air-dried in a ventilated environment, and weighed using a digital balance (Denver instrument P-4002). For flume compartmentalization purposes, wooden and fabric frames were used as shown in Fig. 1e. The experiments were repeated at the beginning of the experimental campaign to check the repeatability, which is satisfactory. Therefore, test repetitions were performed randomly for the rest of the campaign (see supplementary material). For repeated tests, the results refer to the mean values between the repetitions.

2.4. Data Processing

The analysis of wave parameters is divided into two steps. In the first stage, a reflection analysis was carried out to provide the incident wave height for each sea state. The reflection analysis was performed by using 5 wave gauges, WG_{1-5} placed as shown in Fig. 1f, using the procedure described by Andersen et al. (2017)

for regular waves and Eldrup and Andersen (2019) for irregular waves. In the second step, a standard zero-crossing analysis was performed for each free surface elevation time series to quantify the variation of wave parameters along the wave flume.

Cross-shore concentrations (C) of plastic debris were obtained in two ways. On the one hand, the stationary cross-shore distributions were obtained as a percentage by weight from data collection and weighting. On the other hand, the temporal evolution of cross-shore distributions, expressed as a percentage by area, resulted from image processing. Thus, a frame for every four wave periods was extracted from each video and an algorithm based on MATLAB code was applied to identify the positions and measure areas of the different plastic debris at different time instants. Some examples of the ability of algorithms to identify the P3 and P1 plastic debris are shown in Fig. 3. Measurements by weight are used to validate image processing results and quantify the potential overlapping between plastic debris.

2.4.1. Dimensionless variables

In this section the dimensionles variables used within the present study are listed. As far as hydrodynamics is concerned, the dimensionless wave parameter HgT^2 is introduced. This parameter synthetically describes the wave conditions and can be considered a measure of wave steepness (LeMéhauté, 1969; De Leo et al., 2021), varying between 0.008 and 0.002 for W1 and W2, respectively, and being 0.005 ($H_{m0}gT_p^2$) for W3.

Regarding the plastic-debris characteristics, the dimensionless terminal velocities $\omega^*_{s,r}$ are introduced following Dietrich (1982), as a function of dimensional terminal velocity $\omega_{s,r}$, gravitational acceleration g, relative density $R \;\; |\rho_P - \rho_w|\rho_w$, and kinematic viscosity of fluid ν. Finally, two dimensionless variables used to take into account both plastic-debris and wave characteristics are defined, namely Ω and Ω^*:

$$\Omega \;\; \frac{H}{gT^2\omega_s^*}, \tag{1}$$

and

$$\Omega^* \;\; \frac{H\omega_r^*}{gT^2}. \tag{2}$$

These variables relate the steepness of the waves and the buoyancy of plastic materials and, therefore, are useful to describe the input and transport rates of non-buoyant and buoyant plastic debris under different wave conditions.

3. Results

3.1. Hydrodynamic conditions

The results of the reflection analysis provided the following incident wave conditions $H_i^{W1} \;\; 0.184\ m$, $H_i^{W2} \;\; 0.097\ m$, and $H_{m0,i}^{W3} \; 0.097\ m$. From zero-crossing analysis, the average wave heights (H) and the average wave-induced currents (u_{av}) of 50 waves were obtained for the W1 and W2 regular conditions. The W3 irregular condition was characterized by its maximum wave height (H_{max}), H_{m0}, and u_{av} of the set of 1000 waves.

According to the above, the average H_{reg}^{W1} of 18 *cm* registered by WG_1 for the regular wave condition W1 cross-shore propagates and reaches 19.7 *cm* at the WG_8 location (x = 11.7 *m*), where the wave breaks (Fig. 4a). ADVs show average wave-induced currents in an offshore direction (Fig. 4b). At the beginning of the shoaling zone, currents of 2.1 *cms*, 1.8 *cms*, and 0.9 *cms* were recorded by $ADV_{01-0.3}$, respectively. Before wave breaking, these values range between 3.5-5.3 *cms* near the bottom (ADV_{04-05}) and exceed 9 *cms* at the ADV_{06}. ADV_{07} and ADV_{08}, both located near the surface and after wave breaking, recorded average currents of 14.5 *cms* and 12.77 *cms*, respectively.

The wave height records for W2 show that H_{reg}^{W2} increases from 10 *cm* at the WG_1 location, close to the generation area, to 14.7 *cm* at the WG_9 location (x = 13.7 *m*), before wave breaking (Fig. 4a). It was observed that the breaking point occurred at x = 14.3 *m*. The average currents recorded in the shoaling zone range between 0.4-1.0 *cms* (ADV_{01-03}) and between 0.7-4 *cms* (ADV_{04-06}), all in an offshore direction. Average currents near the surface of 3.88 *cms* and 13.9 *cms* were recorded by the ADV_{07} and ADV_{08} locations, respectively, which correspond before and after wave breaking (Fig. 4b).

For the W3 irregular wave condition, the breaking of the largest waves (H_{max}^{W3} 17.2 *cm*) takes place at the WG_8 location (x = 11.7 *m*). H_{m0}^{W3} is close to 10 *cm* from the WG_1 location to the WG_9 location (x = 13.7 *m*), where H_{m0}^{W3} breaks (Fig. 4a). The average recorded wave-induced currents were all offshore below the still sea water level (SWL) (Fig. 4b). The average of the currents recorded by ADV_{01-03} fluctuates between 0.3-1.1 *cms*, while the average of the records of ADV_{04-06} ranges between 0.6-2 *cms*. Average currents of 2.6 *cms* and 5 *cms* were measured in the ADV_{07} and ADV_{08} locations, respectively.

The reflection coefficient provided by AWASYS ranged between 0.11 (W1, W2) and 0.21 (W3), which means that the reflection effect is minimal and corresponds to that of a dissipative beach profile.

3.2. Terminal velocities

The terminal settling and rising velocities were estimated experimentally as the average value of at least five repetitions. Fig. 5a shows the statistics in terms of box plots of these estimates where median (red lines), maximum and minimum (black lines), first and third quartiles (blue boxes), and outlier (red crosses) values are reported (see supplementary material). It is worth noticing that generally the dispersion of these estimates is slight, while larger values are obtained for P13 and P14. Moreover, one outlier was found for P5 and P15, respectively. Furthermore, it is worth to highlight that some secondary movements have been noticed when estimating terminal velocities for large and flexible plastic materials. In order to overcome potential uncertainties in the terminal-velocity estimates, due to the number of repetitions, they were compared with those obtained from the empirical equation proposed by Francalanci et al. (2021) ($\omega_{s,r}^{T}$) as a cross-check of the reliability, although these formulae have not been tested for large and flexible particles. Fig. 5b represents the scatter-plot $\omega_{s,r}$ - $\omega_{s,r}^{T}$, where both data sets show a good agreement with R^2 of 0.98 (Spearman, 1961).

Fig. 5c shows the terminal settling velocities (ω_s) versus nominal diameter (D_n) for plastic debris with a density greater than that of the water. For 2D plastic debris from P1 to P6 (PVC), a larger D_n results in a larger projected area in the direction of motion and in a smaller ω_s. For similar values of D_n, P8 (elastane polyester) shows a slightly higher ω_s than the PVC fragments. This could be because P8, despite having a 20% less density than PVC items, shows a smaller projected area in the direction of motion for the same D_n. Something similar was found for buoyant debris (Fig. 5d). Terminal rising velocities (ω_r) for the 2D LDPE items (from P9 to P12) show lower values the greater the projected surface in the direction of motion. The PP fragments (P14-P15) show higher ω_r, likely due to a smaller projected area for the same D_n and a lower density. Finally, the highest ω_r is obtained for the face masks because their density is 60% lower than that of the rest of the buoyant materials. To sum up, the behavior observed for the 2D or cylindrical elements tested here differs from the behavior of spherical elements. The larger the size, i.e., the larger D_n, the lower terminal velocities characterize these plastic debris, contrary to what happens with spherical elements (e.g., Dietrich, 1982; Francalanci et al., 2021; De Leo et al., 2021).

3.3. Plastic-debris transport and distribution

In order to check the reliability of the image analysis results and to quantify the potential overlapping between plastic debris, a validation was performed by using weight measurements. Fig. 6 shows the comparisons between the stationary distributions, for IC_{shore} (left panel) and $IC_{distributed}$ (right panel), obtained by image analysis (x-axis) and weighting (y-axis). Spearman's R^2 of 0.92 and 0.94, respectively, reports on the high degree of accuracy of the results provided by image processing.

Fig. 7 shows the cross-shore stationary distributions, expressed as a weight percentage, of the 15 types of plastic debris studied under the 3 wave conditions and the two initial conditions for plastic-debris release (IC_{shore} in the upper panels; $IC_{distributed}$ in the lower panels). The order chosen for the plastic debris in this and the following figures follows three levels. From top to bottom, they are first ordered from the highest to the lowest density; the second level of order is from more to less elongated plastic items; and the third level is from the highest to the lowest D_n. The results with IC_{shore} show predominant accumulations of sinking and buoyant plastic debris in the breaking and near-shore zones, respectively. The results with

$IC_{distributed}$ indicate that the waves are not always able of transporting the plastic debris from the offshore zone. It is observed that the greater the steepness of the waves, the greater the transport to the breaking and near-shore zones for sinking and buoyant items, respectively.

In general, the distribution patterns observed for the plastic materials are consistent with the undertow profiles observed in the laboratory. The mass transport of the undertow profile that characterizes the surf zone generates an onshore transport for the buoyant materials that accumulate near the beach. On the contrary, those heavy plastics that the waves managed to put into suspension were transported by the undertow current until the beginning of the breaking zone, where the energy of the waves is small enough to allow the plastic to settle. This zone coincides with the area where the typical barrier of erosive or offshore processes arises.

Fig. 8 shows the temporal evolution of concentrations when plastic debris was released into the wave flume from the run-up zone. It was found that plastic materials with a density greater than that of the water (from P1 to P6 and P8) that manage to escape entrapment on the beach tend to be transported to the breaking zone. Inertial effects play an important role in this behavior, i.e., whether plastic debris manages to escape this coastal entrapment depends not only on wave conditions but also on the features of plastic debris that define its position in the water column. A higher escape rate was found for plastic materials with higher settling velocities and in less-steep sea states, indicating that escapement occurs primarily close to the bottom. Nevertheless, the input rates of elongated plastic items (from P4 to P6) mainly depend on the initial arrangement between the items. If the degree of packing is high on the shore, elongated items link together to make up a new elemental unit that is transported by the waves to the run-up limit, where they remain trapped. However, if the degree of packing is low, they behave like the less elongated elements and are transported to the breaking zone where they accumulate. The buoyant debris (P7 and from P9 to P15) is mostly retained near the shore, distributed between the surf and beach areas. However, it was observed that those materials with lower buoyancy (from P9 to P11) under wave conditions with lower HgT^2 (W2 and W3) could escape to the breaking zone and even to the shoaling zone (W2). Regarding this relationship between the input rates of plastic debris from the beach to the marine environment and the wave conditions, in general, a greater escape rate of plastic debris is observed for W2—the wave condition with the lowest HgT^2—since long waves, cause less breaking, and more intense offshore current near the shoreline, as can be seen in Fig. 4.

Fig. 9 shows the relationship between the dimensionless parameters Ω and Ω^* and the final escape rates (E) for plastic debris with a density greater and smaller than that of the water (left and right panels, respectively). The results indicate that the lower the buoyancy of plastic debris, i.e., the higher ω_s^* for elements with a density greater than that of the water and the lower ω_r^* for elements with a density lower than that of the water, and the lower the wave parameter HgT^2, the higher the percentage of plastic debris that escapes coastal entrapment. It was found that values of Ω and Ω^* less than 0.0075 and 0.0025, respectively, favor an escape rate of plastic debris from the beach greater than 50%.

These findings provide a first insight related to the beaching effect. Tab. 2 collects the $\omega_{s,r}^*$ and final percentages trapped on the beach (β) for the irregular wave condition W3 and each type of plastic debris under study. The experimental results point out this relationship between $\omega_{s,r}^*$, the degree of packing for the elongated items, and beaching. Except for elongated debris types with a high degree of packing, if ω_s^* is lower than unity (such as P3), the percentage that remains trapped on the beach is equal to or greater than 50%; while if ω_s^* is greater than 1 (all other analyzed plastic types with densities greater than that of the water), the trapped percentage can be neglected (<10%). For buoyant items, ω_r^* greater than 1 (P7 and from P13 to P15) and lower than 1 (from P9 to P12) characterize trapping above and below 50%, respectively. This behavior may be related to that the more buoyant the materials are, the more they are affected by mass transport near the surface due to breaking.

Fig. 10 shows the temporal evolution of concentrations of plastic materials when they are initially released along the wave flume following a uniform distribution. In general, plastic materials with densities greater than that of the water were transported and accumulated in the breaking zone, while elements of lower density were transported and accumulated near the beach. Fig. 11 shows the relationship between the final concentrations in the breaking and beach areas for plastic debris with a density greater and smaller than that of the water and the parameters Ω and Ω^*, respectively. Higher transport rates were found for the materials that acquired positions in the water column closer to the surface (lower ω_s and higher ω_r) for wave conditions with higher HgT^2. Ω and Ω^* greater than 0.0025 and 0.0075, respectively, favor transports and accumulations greater than 50% in the breaking and beach areas for non-buoyant and buoyant plastic elements, respectively.

4. Discussion

4.1. Plastic-debris characteristics

The plastic debris under study involves fragments of polypropylene, polyethylene, polystyrene, and PVC of different sizes and shapes, as well as face masks. This selection is intended to cover a wide range of densities, sizes, and shapes of plastic debris, since these are characteristics that play an important role in plastic-debris buoyancy, i.e., in defining its position in the water column, and therefore make it be affected by different transport mechanisms. The results observed in this experiment agree with previous findings and show that lightweight macroplastics and mesoplastics (e.g., face masks) are transported on the surface by waves, heavier plastics (e.g., PVC) are predominantly deposited on the bottom near the breaking zone, while microplastics are mainly transported as suspended particles and its onshore transport increases with buoyancy (Filella, 2015; Zhang, 2017). The shape is also significative, for instance, heavier 2D shapes usually show greater buoyancy than spheres with the same density and volume (Chubarenko and Stepanova, 2017).

4.2. Initial release of plastic debris

The results derived from the initial condition of plastic materials in the run-up zone provide information on their input rate into the marine environment, as well as on their transport and distribution from the coast. This is an important and novel topic considering that sources of plastic debris were primarily land-based and attributed to coastal recreational activities (Lee et al., 2013; Rech et al., 2014; Galgani et al., 2015). It was found that plastic materials with greater sinking ability were more likely to enter the water environment from the beach, especially for wave conditions with low HgT^2. Note that small values of HgT^2 may refer to two different transport conditions: low-energy wave conditions (e.g., towards the end of a storm when debris tend to be beached, see Chubarenko and Stepanova, 2017) and long-wave conditions (i.e., large wave period, where strong and prolonged in time currents occur).Moreover, it was observed that if there was a high concentration of elongated plastic items on the coast, they remain trapped on the beach until other processes, such as wind or degradation manage to undo that new unit they formed (Isobe et al., 2014; Critchell and Lambrechts, 2016). It should be noted that only two qualitative degree of packing were investigated in this study, namely high and low. Further studies exploring different configurations for different types of plastic debris are needed to extend the applicability of the results to natural conditions, where plastic items interact with each other and/or with sediment grains, sea weeds or nets.

Furthermore, some preliminary beaching aspects for the plastic debris under study were derived from this initial arrangement on the run-up zone. It was observed, the more buoyant the materials, the more likely they are to remain stranded on shoreline affected by mass transport near the surface due to breaking. Nevertheless, since the beach profile in the laboratory was made on a methacrylate background, which naturally does not constitute any substrate, further *ad hoc* field and laboratory studies are needed to gain insight on the entrapment processes between different types of shorelines (e.g., with or without vegetation, sand, mud, etc.) and different types of plastic debris (Núñez et al., 2019; Van Sebille et al., 2020). Moreover, it should be highlighted that real bathymetry, bed roughness and presence of bottom forms (and their changes in space and time) are expected to modify the hydrodynamics and therefore the transport and dispersion of plastic debris.

The results with the initial conditions of plastic debris uniformly distributed along the wave flume indicated that, contrary to what happens with the input entry from the beach, a greater transport originates for the more buoyant materials and under the wave conditions with large HgT^2. This aspect became especially relevant in the offshore zone, which could be due to the Stokes drift (Isobe et al., 2014; Zhang, 2017; Stocchino et al., 2019; Alsina et al., 2020). Regarding the sinking materials, they are transported by the residual current at the bottom to the breaking point, which is in agreement with the findings of Forsberg et al. (2020).

4.3. Regular/Irregular waves

Another relevant and novel aspect included in this research is the influence of irregular waves. It was found that the irregular wave condition W3, whose target signal is characterized by a H_{max}^{W3} of 18 *cm* similar to H_{reg}^{W1} and a H_{m0}^{W3} of 10 *cm* equal to H_{reg}^{W2}, allowed plastic debris to escape from the beach area at times corresponding to the lowest wave heights. Thus, the percentage of each plastic debris that managed to escape from the beach at the end of this irregular sea state showed intermediate values between the percentages associated with the regular conditions W1, which showed the greatest entrapment rates, and W2, which showed the lowest entrapment rates. An average behavior was also found in transport under W3 compared to W1 and W2. It can be deduced from these experimental results that the final cross-shore distribution of plastic debris is similar under regular and irregular sea states; however, cross-shore transport processes are affected by the different time scales associated with regular and irregular wave conditions, as is the case with beach profiles (Dean, 1985; Kerpen et al., 2020).

4.4. Dimensional scaling

When conducting laboratory experiments, challenges related to dimensional scaling are almost inevitable (Forsberg et al., 2020). As is well known, the problems of evaluating plastic debris transport in laboratory-scale tests are like those arising when evaluating sediment transport, due to the difficulty of scaling viscous and inertial forces. In this study, no specific scale factor was selected since basic hydrodynamic phenomena and no specific case/configuration are reproduced,i.e., the behavior of plastic debris under small waves was assessed. Further studies on a larger scale are needed to be able to extend the conclusions derived from these experiments.

4.5. Terminal velocity

The terminal velocity estimate in this study show some uncertainties and limitations. First, the number of repetitions to quantify the terminal velocity should be high enough to reduce the related uncertainties (Kaiser et al., 2017), while in this study only five (six in some cases) repetitions have been performed. Second, the Francalanci's formulae (Francalanci et al., 2021), valid for a wide range of plastic shapes (3D, 2D, and 1D) and compositions in quiescent fluids, have been used as a cross-check of the reliability of these estimates, although these formulae have not been tested for large and flexible particles. Moreover, some simplifications have been assumed: I) terminal velocity estimates in calm water is physically interpreted by considering simple physical parameters of plastic materials (i.e., density and projected areas), without analyzing in-depth other relevant processes (see Chubarenko et al., 2016). This approach is intended to be appropriate for an aggregate interpretation of the input/transport rates of plastic debris; II) terminal velocities are estimated in calm water. This is obviously a simplification, because turbulence processes induced by waves may affect the terminal velocity, as demonstrated by De Leo et al. (2021). To summarize, terminal velocity is a key factor controlling the vertical distribution of plastic debris and, therefore, its wave-induced transport (Van Sebille et al., 2020), nevertheless, the aggregate description of the cross-shore distribution/accumulation pattern of plastic debris (i.e., the objective of the paper) is not expected to be affected by these uncertainties/simplifications in the terminal velocity.

4.6. Salinity and biofouling

The results observed during laboratory tests would be significantly altered by the presence of salinity in the water, which is naturally present in the marine environment. Due to technical reasons, the experiments were performed using fresh water. Therefore, it is expected that the behavior of plastic materials will be modified, with special significance for those whose density is between that of fresh water and that of seawater (Forsberg et al., 2020). For instance, the transport of the P8 test material, with a density of 1020 kgm^3, would change from sinking to floating. Nevertheless, the behavior of any type of plastic debris could be extrapolate in the natural environment by estimating its settling/buoyancy rate in saline fluids according to the literature.

Another significant mechanism that may also affect the relative densities of plastic debris and consequently their transport and dispersion patterns is biofouling, which could even sink the least dense plastic materials (Andrady, 2011; Chubarenko et al., 2016; Fazey and Ryan, 2016; Kaiser et al., 2017; Van Sebille et al., 2020). Further research is needed to gain insight into the changes that biofouling growth can produce in the specific density of plastic materials and, consequently, be able to infer their transport and dispersion patterns.

4.7. *On the validation of predictive tools*

A new and significant database is generated that expands the laboratory findings collected by the state-of-the-art on the transport and dispersion of plastic debris in the near-shore zone under the wave and wind action (Forsberg et al., 2020; Kerpen et al., 2020; De Leo et al., 2021). This extended database is relevant for the Scientific Community to validate and improve numerical modeling of plastic debris transport (e.g., Núñez et al., 2019; Jalón-Rojas et al., 2019).

The predictive tool would consist of coupling a hydrodynamic model, e.g., IHFOAM (Lara et al., 2008, 2011; Higuera et al., 2013a,b) or SWASH (Zijlema et al., 2011), and a Lagrangian tracking model, e.g., Ocean Parcels (van Sebille et al., 2018), TESEO (Abascal et al., 2007), MOHID (Braunschweig et al., 2003; de Pablo et al., 2020), which would be fed by the hydrodynamic one. The extended experimental database is made of hydrodynamic and trajectory data and, therefore, can be used to validate both the hydrodynamic and the Lagrangian transport models. The validated numerical tool will allow to address some of the relevant issues that have not been included to date. Thus, numerical studies to explore the influence of new wind and wave conditions that are impossible to analyze with the limitations of the laboratory, new beach profiles, or new types of plastic debris with or without biofouling growth immersed in fluids with different salinities could be included. It would even be possible to make the leap from cross-shore (2DV) to 3D physics of plastic debris and, for instance, address the effect of longshore currents on the nearshore transport and dispersion.

5. Conclusions

This research studies novel aspects of the cross-shore transport of plastic debris in the breaking zone. The behavior of micro, meso, and macroplastic with densities greater and smaller than that of the water with two-dimensional, such as face masks, and cylindrical shapes under regular and irregular wave conditions was analyzed. In addition to assessing the transport and dispersion of plastic debris present in the marine environment, the study of the input rate of plastic debris from land to sea was included as a new issue. With this aim, two parameters Ω and Ω^*, which relate plastic-debris features and wave characteristics, were defined to describe the input and transport rates of plastic debris with a density greater and smaller than that of the water, respectively. The results of this research extend previous findings on microplastic transport in the nearshore zone to new shapes, densities, and sizes of plastic debris.

As for the input rates of plastic debris into coastal waters, higher rates were found for the lowest wave parameters HgT^2 (i.e., strong current conditions due to large wave periods) and plastic items that show a greater tendency to sink. The sinking ability of plastic debris depends on its terminal velocities. Terminal velocities are greater the greater the difference between the densities of plastic debris and the density of water and the smaller the area of plastic debris projected in the direction of motion. That is, the plastic debris considered in this study having a density greater than that of the water show a greater ability to escape the greater their density, the smaller their projected area and, therefore, the greater their settling rate; while buoyant elements with the greatest probability of escaping are those that show a greater projected surface. For the elongated plastic items, the input rate was found to depend on the initial arrangement between them. If the initial arrangement on the beach is with a low concentration of elongated items, the behavior does not change and the input rate depends on the sinking ability and the steepness of waves. On the contrary, items join if the degree of packing on land is high and are transported by waves to the limit of run-up, where they remain trapped. It was found that values of Ω and Ω^* less than 0.0075 and 0.0025, respectively, favor an escape rate of plastic debris from the beach greater than 50%.

Regarding the transport and dispersion of plastic debris that is already present in the marine environment, higher transport rates were observed for the most buoyant elements and higher wave parameters HgT^2, generating a predominant accumulation in the breaking area for materials with a density greater than that of the water and closer to the shore for the more buoyant plastic debris. Ω and Ω^* greater than 0.0025 and 0.0075, respectively, favor transport and accumulation greater than 50% in the breaking and beach areas for non-buoyant and buoyant plastic materials, respectively.

To sum up, wave characteristics together with densities, shapes, and sizes of plastic debris determine its terminal velocities, its position in the water column, and, therefore, its entry, transport, and distribution in the marine environment.

6. Acknowledgments

P.N. is supported by a Margarita Salas post-doctoral fellowship funded by European Union-NextGenerationEU, Ministry of Universities and Recovery Transformation and Resilience Plan, through a call from the University of Cantabria. The financial support from the Government of Cantabria through the FÉNIX Program (ID 2020.03.03.322B.742.09) is warmly acknowledged. We acknowledge M.S. and the IHLab-Hydro team for all the technical support.

Appendix A Supplementary material

Supplementary data to this article are provided.

References

Abascal, A.J., Castanedo, S., Gutierrez, A.D., Comerma, E., Medina, R., Losada, I.J., 2007. Teseo, an operational system for simulating oil spills trajectories and fate processes, in: The Seventeenth International Offshore and Polar Engineering Conference, OnePetro.

Abascal, A.J., Castanedo, S., Medina, R., Losada, I.J., Alvarez-Fanjul, E., 2009a. Application of hf radar currents to oil spill modelling. Marine pollution bulletin 58, 238–248.

Abascal, A.J., Castanedo, S., Mendez, F.J., Medina, R., Losada, I.J., 2009b. Calibration of a lagrangian transport model using drifting buoys deployed during the prestige oil spill. Journal of Coastal Research 25, 80–90.

Alsina, J.M., Jongedijk, C.E., van Sebille, E., 2020. Laboratory Measurements of the Wave-Induced Motion of Plastic Particles: Influence of Wave Period, Plastic Size and Plastic Density. Journal of Geophysical Research: Oceans 125, e2020JC016294.

Andersen, T.L., Eldrup, M.R., Frigaard, P., 2017. Estimation of incident and reflected components in highly nonlinear regular waves. Coastal Engineering 119, 51–64.

Andrady, A.L., 2011. Microplastics in the marine environment. Marine pollution bulletin 62, 1596–1605.

Bandi, M., 2020. Electrocharged facepiece respirator fabrics using common materials. Proceedings of the Royal Society A 476, 20200469.

Barnes, D., Galgani, F., Thompson, R., Barlaz, M., 2009. Accumulation and fragmentation of plastic debris in global environments. Philosophical Transactions of the Royal Society B: Biological Sciences 364, 1985–1998.

Braunschweig, F., Martins, F., Chambel, P., Neves, R., 2003. A methodology to estimate renewal time scales in estuaries: the tagus estuary case. Ocean Dynamics 53, 137–145.

Browne, M.A., Galloway, T.S., Thompson, R.C., 2010. Spatial patterns of plastic debris along estuarine shorelines. Environmental science & technology 44, 3404–3409.

Cardenas, M., Abascal, A., Castanedo, S., Chiri, S., Ferrer, M., Sanchez, J., Medina, R., Turrell, W., Hughes, S., Gallego, A., et al., 2015. Spill trajectory modeling based on hf radar currents in the north sea: Validation with drifter buoys, in: Proc. of the Thirty Eighth AMOP Technical Seminar, Vancouver, BC, Canada, Jun, pp. 123–142.

Chubarenko, I., Bagaev, A., Zobkov, M., Esiukova, E., 2016. On some physical and dynamical properties of microplastic particles in marine environment. Marine pollution bulletin 108, 105–112.

Chubarenko, I., Stepanova, N., 2017. Microplastics in sea coastal zone: Lessons learned from the baltic amber. Environmental pollution 224, 243–254.

Corey, A.T., 1949. Influence of shape on the fall velocity of sand grains. Ph.D. thesis. Colorado A & M College.

Crawford, C., Quinn, B., 2017. 5-microplastics, standardisation and spatial distribution. Microplastic Pollutants; Elsevier: Kidlington, UK , 101–130.

Critchell, K., Lambrechts, J., 2016. Modelling accumulation of marine plastics in the coastal zone; what are the dominant physical processes? Estuarine, Coastal and Shelf Science 171, 111–122.

Cunningham, H., Higgins, C., van den Bremer, T., 2022. The role of the unsteady surface wave-driven Ekman–Stokes flow in the accumulation of floating marine litter. Journal of Geophysical Research: Oceans 127, e2021JC018106.

De Leo, A., Cutroneo, L., Sous, D., Stocchino, A., 2021. Settling Velocity of Microplastics Exposed to Wave Action. Journal of Marine Science and Engineering 9, 142.

Dean, R., 1985. Physical modelling of littoral processes, in: Physical modelling in coastal engineering. R.A. Dalrymple (Newark, DE: Balkema), pp. 119–139.

Derraik, J., 2002. The pollution of the marine environment by plastic debris: a review. Marine pollution bulletin 44, 842–852.

Dietrich, W.E., 1982. Settling velocity of natural particles. Water resources research 18, 1615–1626.

Eldrup, M.R., Andersen, T.L., 2019. Estimation of incident and reflected wave trains in highly nonlinear two-dimensional irregular waves. Journal of Waterway, Port, Coastal, and Ocean Engineering 145, 04018038.

van Emmerik, T., de Lange, S., Frings, R., Schreyers, L., Aalderink, H., Leusink, J., Begemann, F., Hamers, E., Hauk, R., Janssens, N., Jansson, P., Joosse, N., Kelder, D., van der Kuijl, T., Lotcheris, R., Löhr, A., Mellink, Y., Pinto, R., Tasseron, P., Vos, V., Vriend, P., 2022. Hydrology as a driver of floating river plastic transport. Earth's Future 10, e2022EF002811.

Fazey, F.M., Ryan, P.G., 2016. Biofouling on buoyant marine plastics: An experimental study into the effect of size on surface longevity. Environmental pollution 210, 354–360.

Filella, M., 2015. Questions of size and numbers in environmental research on microplastics: methodological and conceptual aspects. Environmental Chemistry 12, 527–538.

Forsberg, P.L., Sous, D., Stocchino, A., Chemin, R., 2020. Behaviour of plastic litter in nearshore waters: First insights from wind and wave laboratory experiments. Marine pollution bulletin 153, 111023.

Francalanci, S., Paris, E., Solari, L., 2021. On the prediction of settling velocity for plastic particles of different shapes. Environmental Pollution 290, 118068.

Galgani, F., Hanke, G., Maes, T., 2015. Global distribution, composition and abundance of marine litter, in: Marine anthropogenic litter. Springer, Cham, pp. 29–56.

Galgani, F., Hanke, G., Werner, S., De Vrees, L., 2013. Marine litter within the European marine strategy framework directive. ICES Journal of Marine Science 70, 1055–1064.

Gallo, F., Fossi, C., Weber, R., Santillo, D., Sousa, J., Ingram, I., Nadal, A., Romano, D., 2018. Marine litter plastics and microplastics and their toxic chemicals components: the need for urgent preventive measures. Environmental Sciences Europe 30, 1–14.

Galloway, T.S., Cole, M., Lewis, C., 2017. Interactions of microplastic debris throughout the marine ecosystem. Nature ecology & evolution 1, 1–8.

Gurumoorthi, K., Suneel, V., Rao, V.T., Thomas, A.P., Alex, M., 2021. Fate of MV Wakashio oil spill off Mauritius coast through modelling and remote sensing observations. Marine Pollution Bulletin 172, 112892.

Hardesty, B.D., Harari, J., Isobe, A., Lebreton, L., Maximenko, N., Potemra, J., Van Sebille, E., Vethaak, A.D., Wilcox, C., 2017. Using numerical model simulations to improve the understanding of micro-plastic distribution and pathways in the marine environment. Frontiers in marine science 4, 30.

Heo, N.W., Hong, S.H., Han, G.M., Hong, S., Lee, J., Song, Y.K., Jang, M., Shim, W.J., 2013. Distribution of small plastic debris in cross-section and high strandline on Heungnam beach, South Korea. Ocean Science Journal 48, 225–233.

Higuera, P., Lara, J.L., Losada, I.J., 2013a. Realistic wave generation and active wave absorption for Navier–Stokes models: Application to OpenFOAM®. Coastal Engineering 71, 102–118.

Higuera, P., Lara, J.L., Losada, I.J., 2013b. Simulating coastal engineering processes with OpenFOAM®. Coastal Engineering 71, 119–134.

Isobe, A., Kubo, K., Tamura, Y., Nakashima, E., Fujii, N., 2014. Selective transport of microplastics and mesoplastics by drifting in coastal waters. Marine pollution bulletin 89, 324–330.

Jalón-Rojas, I., Wang, X.H., Fredj, E., 2019. A 3D numerical model to track marine plastic debris (TrackMPD): sensitivity of microplastic trajectories and fates to particle dynamical properties and physical processes. Marine pollution bulletin 141, 256–272.

Jambeck, J., Geyer, R., Wilcox, C., Siegler, T., Perryman, M., Andrady, A., Narayan, R., Law, K., 2015. Plastic waste inputs from land into the ocean. Science 347, 768–771.

Kaiser, D., Kowalski, N., Waniek, J.J., 2017. Effects of biofouling on the sinking behavior of microplastics. Environmental research letters 12, 124003.

Kako, S., Isobe, A., Kataoka, T., Hinata, H., 2014. A decadal prediction of the quantity of plastic marine debris littered on beaches of the East Asian marginal seas. Marine pollution bulletin 81, 174–184.

Kako, S., Isobe, A., Magome, S., Hinata, H., Seino, S., Kojima, A., 2011. Establishment of numerical beach-litter hindcast/forecast models: An application to Goto Islands, Japan. Marine pollution bulletin 62, 293–302.

Kerpen, N.B., Schlurmann, T., Schendel, A., Gundlach, J., Marquard, D., Hüpgen, M., 2020. Wave-induced distribution of microplastic in the surf zone. Frontiers in Marine Science 7, 979.

Komar, P.D., Reimers, C., 1978. Grain shape effects on settling rates. The Journal of Geology 86, 193–209.

Kukulka, T., Proskurowski, G., Morét-Ferguson, S., Meyer, D.W., Law, K.L., 2012. The effect of wind mixing on the vertical distribution of buoyant plastic debris. Geophysical Research Letters 39.

Lara, J., Losada, I., Guanche, R., 2008. Wave interaction with low-mound breakwaters using a RANS model. Ocean engineering 35, 1388–1400.

Lara, J.L., Ruju, A., Losada, I.J., 2011. Reynolds averaged Navier-Stokes modelling of long waves induced by a transient wave group on a beach. Proceedings of the Royal Society A: Mathematical, Physical and Engineering Sciences 467, 1215–1242.

Law, K., Morét-Ferguson, S., Maximenko, N., Proskurowski, G., Peacock, E., Hafner, J., Reddy, C., 2010. Plastic accumulation in the North Atlantic subtropical gyre. Science 329, 1185–1188.

Lebreton, L.M., Greer, S., Borrero, J., 2012. Numerical modelling of floating debris in the world's oceans. Marine pollution bulletin 64, 653–661.

Lee, J., Hong, S., Song, Y.K., Hong, S.H., Jang, Y.C., Jang, M., Heo, N.W., Han, G.M., Lee, M.J., Kang, D., et al., 2013. Relationships among the abundances of plastic debris in different size classes on beaches in South Korea. Marine pollution bulletin 77, 349–354.

LeMéhauté, B., 1969. An introduction to hydrodynamics and water waves. volume 52. Environmental Science Servies Administration.

Maximenko, N., Hafner, J., Niiler, P., 2012. Pathways of marine debris derived from trajectories of Lagrangian drifters. Marine pollution bulletin 65, 51–62.

Mazarrasa, I., Puente, A., Núñez, P., García, A., Abascal, A., Juanes, J., 2019. Assessing the risk of marine litter accumulation in estuarine habitats. Marine pollution bulletin 144, 117–128.

Middleton, G.V., Southard, J.B., 1978. Mechanics of sediment movement: Lecture notes for short course No. 3. 3, Society of Economic Paleontologists and Mineralogists.

Monismith, S.G., 2020. Stokes drift: theory and experiments. Journal of Fluid Mechanics 884.

Naz, S., Iqbal, M.F., Mahmood, I., Allam, M., 2021. Marine oil spill detection using synthetic aperture radar over Indian Oean. Marine Pollution Bulletin 162, 111921.

Núñez, P., Castanedo, S., Medina, R., 2020. A Global Classification of Astronomical Tide Asymmetry and Periodicity Using Statistical and Cluster Analysis. Journal of Geophysical Research: Oceans 125, e2020JC016143.

Núñez, P., Castanedo, S., Medina, R., 2021. Role of ocean tidal asymmetry and estuarine geometry in the fate of plastic debris from ocean sources within tidal estuaries. Estuarine, Coastal and Shelf Science , 107470.

Núñez, P., García, A., Mazarrasa, I., Juanes, J.A., Abascal, A.J., Méndez, F., Castanedo, S., Medina, R., 2019. A methodology to assess the probability of marine litter accumulation in estuaries. Marine pollution bulletin 144, 309–324.

de Pablo, H., Garaboa-Paz, D., Canelas, R., Campuzano, F., Neves, R., 2020. Mohid-lagrangian: A lagrangian transport model from local to globals scales. applications to the marine litter problem., in: EGU General Assembly Conference Abstracts, p. 21895.

Rech, S., Macaya-Caquilpán, V., Pantoja, J., Rivadeneira, M., Madariaga, D.J., Thiel, M., 2014. Rivers as a source of marine litter–a study from the SE Pacific. Marine pollution bulletin 82, 66–75.

Reisser, J., Slat, B., Noble, K., Du Plessis, K., Epp, M., Proietti, M., de Sonneville, J., Becker, T., Pattiaratchi, C., 2015. The vertical distribution of buoyant plastics at sea: an observational study in the North Atlantic Gyre. Biogeosciences 12, 1249–1256.

Romano, A., Bellotti, G., Briganti, R., Franco, L., 2015. Uncertainties in the physical modelling of the wave overtopping over a rubble mound breakwater: The role of the seeding number and of the test duration. Coastal Engineering 103, 15–21.

Sadri, S.S., Thompson, R.C., 2014. On the quantity and composition of floating plastic debris entering and leaving the Tamar Estuary, Southwest England. Marine pollution bulletin 81, 55–60.

van Sebille, E., Lange, M., Delandmeter, P., 2018. Making virtual particles behave like plastic: developing the oceanparcels lagrangian ocean analysis framework, in: 2018 Ocean Sciences Meeting, AGU.

Spearman, C., 1961. The proof and measurement of association between two things. .

Stocchino, A., De Leo, F., Besio, G., 2019. Sea waves transport of inertial microplastics: Mathematical model and applications. Journal of Marine Science and Engineering 7, 467.

Stringham, G.E., Simons, D.B., Guy, H.P., 1969. The behavior of large particles falling in quiescent liquids. US Government Printing Office.

De-la Torre, G.E., Aragaw, T.A., 2021. What we need to know about PPE associated with the COVID-19 pandemic in the marine environment. Marine pollution bulletin 163, 111879.

Van Sebille, E., Aliani, S., Law, K.L., Maximenko, N., Alsina, J.M., Bagaev, A., Bergmann, M., Chapron, B., Chubarenko, I., Cózar, A., et al., 2020. The physical oceanography of the transport of floating marine debris. Environmental Research Letters 15, 023003.

Van Sebille, E., England, M., Froyland, G., 2012. Origin, dynamics and evolution of ocean garbage patches from observed surface drifters. Environmental Research Letters 7, 044040.

Villarrubia-Gómez, P., Cornell, S.E., Fabres, J., 2018. Marine plastic pollution as a planetary boundary threat–The drifting piece in the sustainability puzzle. Marine policy 96, 213–220.

Wang, W., Ndungu, A.W., Li, Z., Wang, J., 2017. Microplastics pollution in inland freshwaters of China: a case study in urban surface waters of Wuhan, China. Science of the Total Environment 575, 1369–1374.

Yoon, J.H., Kawano, S., Igawa, S., 2010. Modeling of marine litter drift and beaching in the Japan Sea. Marine pollution bulletin 60, 448–463.

Zambianchi, E., Iermano, I., Suaria, G., Aliani, S., 2014. Marine litter in the Mediterranean Sea: an oceanographic perspective, in: CIESM Workshop Monograph 46: Marine litter in the Mediterranean and Black Seas, CIESM Publisher Monaco. pp. 31–41.

Zambianchi, E., Trani, M., Falco, P., 2017. Lagrangian transport of marine litter in the Mediterranean Sea. Frontiers in Environmental Science 5, 5.

Zhang, H., 2017. Transport of microplastics in coastal seas. Estuarine, Coastal and Shelf Science 199, 74–86.

Zijlema, M., Stelling, G., Smit, P., 2011. SWASH: An operational public domain code for simulating wave fields and rapidly varied flows in coastal waters. Coastal Engineering 58, 992–1012.

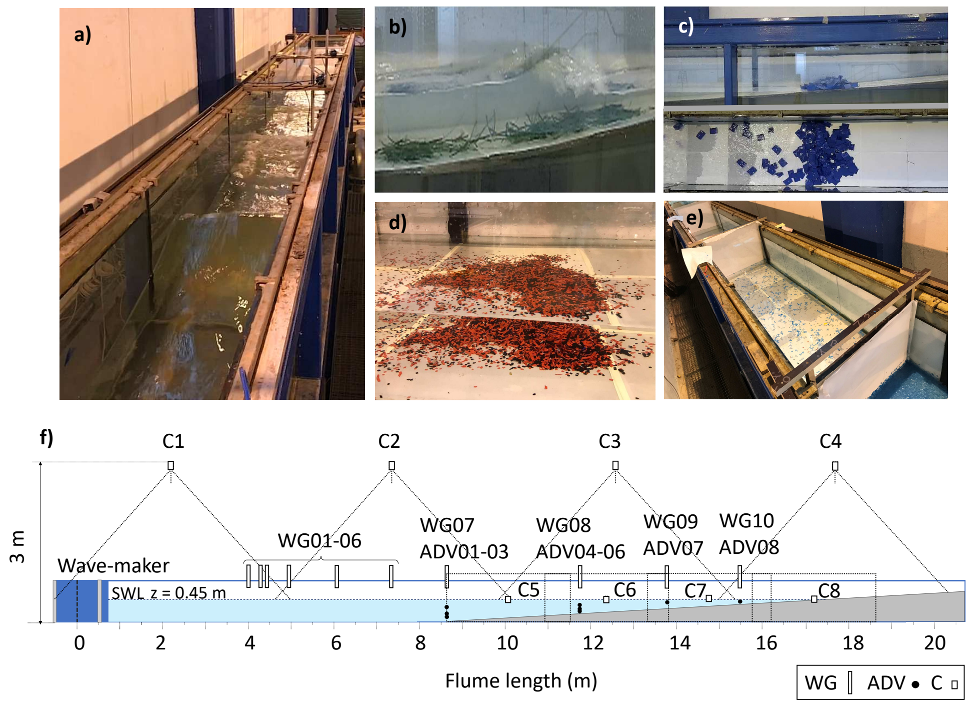

Figure 1: Sketch of the experiments: a) an overview of the wave flume, b-c-d) some of the plastic materials under study, e) wooden and fabric frames to delimit the offshore, shoaling, breaking, surf, and beach areas of the flume, and f) the experimental set-up with wave-gauges (WG), Acoustic Doppler Velocimeters (ADVs), and zenithal/lateral cameras (C).

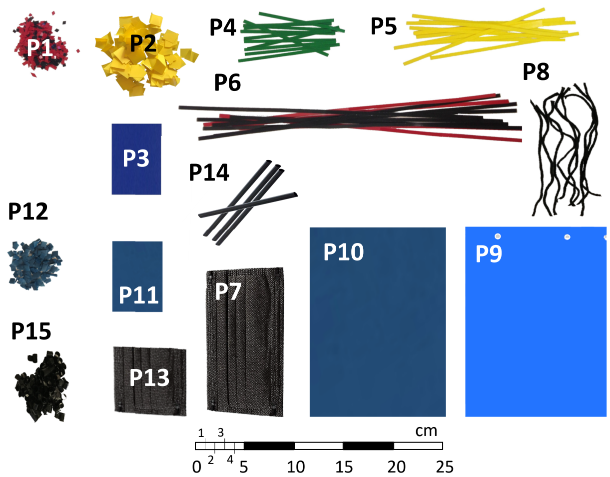

Figure 2: Plastic debris types (P_i) under study.

	ρ_P kgm^3	a m	b m	c m	csf $-$	D_n m
P1	1340	0.0049	0.0049	0.00015	0.0306	0.0015
P2	1340	0.0136	0.0136	0.00015	0.0110	0.0029
P3	1340	0.0750	0.0500	0.00015	0.0024	0.0079
P4	1340	0.1080	0.0049	0.00015	0.0065	0.0042
P5	1340	0.1625	0.0049	0.00015	0.0053	0.0048
P6	1340	0.3250	0.0049	0.00015	0.0038	0.0060
P8	1020	0.1800	0.0020	0.00200	0.1054	0.0029
P9	910	0.2100	0.1485	0.00012	0.0007	0.0148
P10	910	0.2100	0.1485	0.00007	0.0004	0.0123
P11	910	0.0800	0.0550	0.00007	0.0011	0.0065
P12	910	0.0049	0.0049	0.00007	0.0143	0.0012
P14	900	0.1080	0.0030	0.00020	0.1667	0.0041
P15	900	0.0050	0.0030	0.00020	0.7746	0.0015
P7	380	0.1750	0.0950	0.00150	0.0116	0.0284
P13	380	0.0950	0.0875	0.00150	0.0165	0.0226

Table 1: Main features of the plastic debris under study: density (ρ_P), longest axis (a), intermediate axis (b), thickness (c), Corey shape factor (csf), and equivalent nominal diameter (D_n).

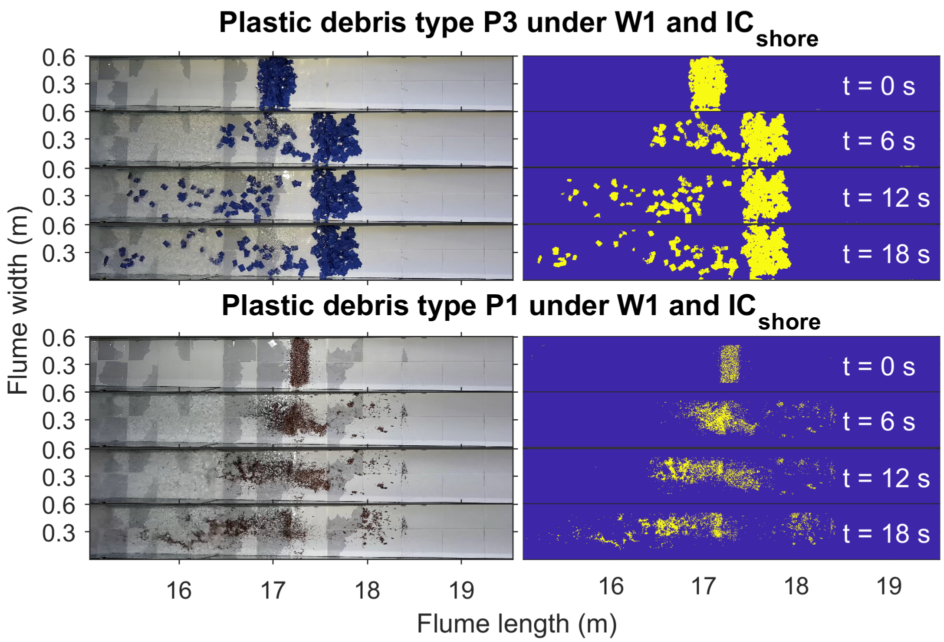

Figure 3: Some results of plastic-debris identification algorithms.

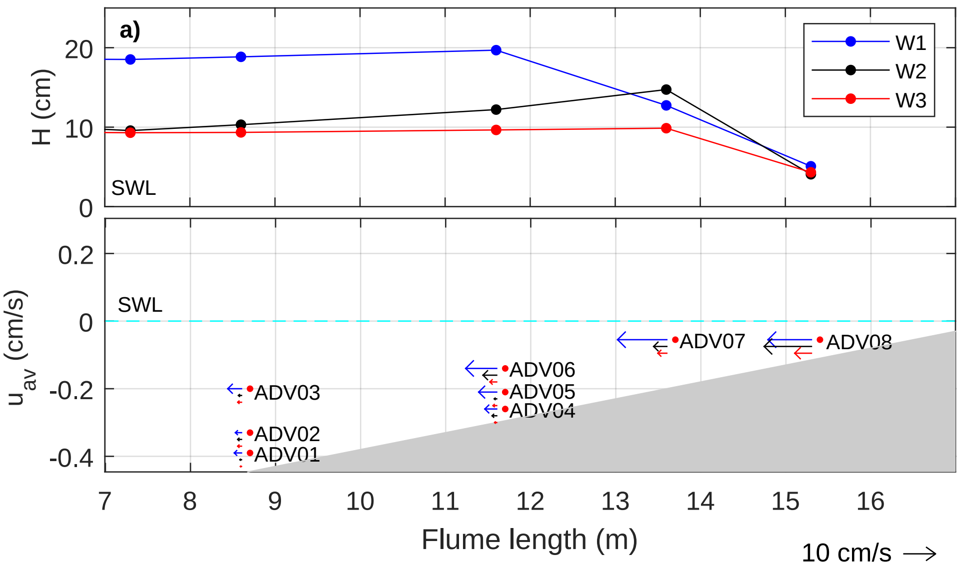

Figure 4: Hydrodynamic conditions W1, W2, and W3 in the shoaling, breaking, and surf zones: a) cross-shore evolution of the wave height (average H for W1-W2; H_{m0} for W3) and b) average wave-induced currents (u_{av}).

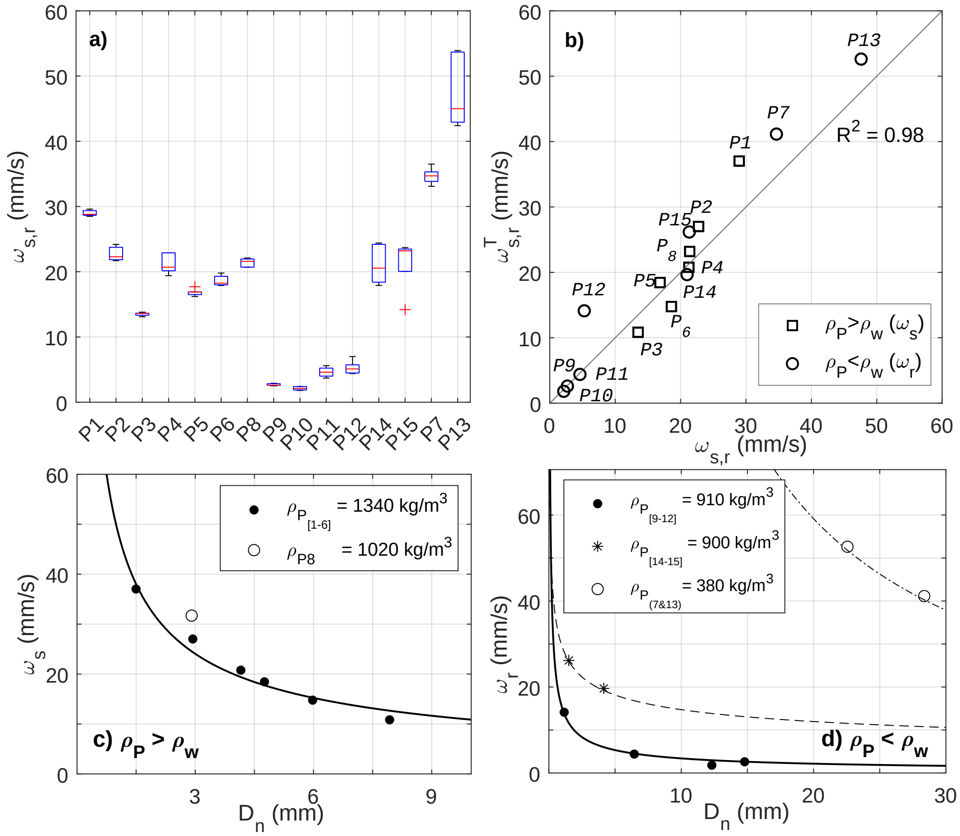

Figure 5: Terminal-velocity estimates: a) box plots (at least five repetitions); b) scatter plot between terminal velocities estimated experimentally ($\omega_{s,r}$) and theoretically ($\omega^T_{s,r}$); c) ω_s versus D_n; d) ω_r versus D_n.

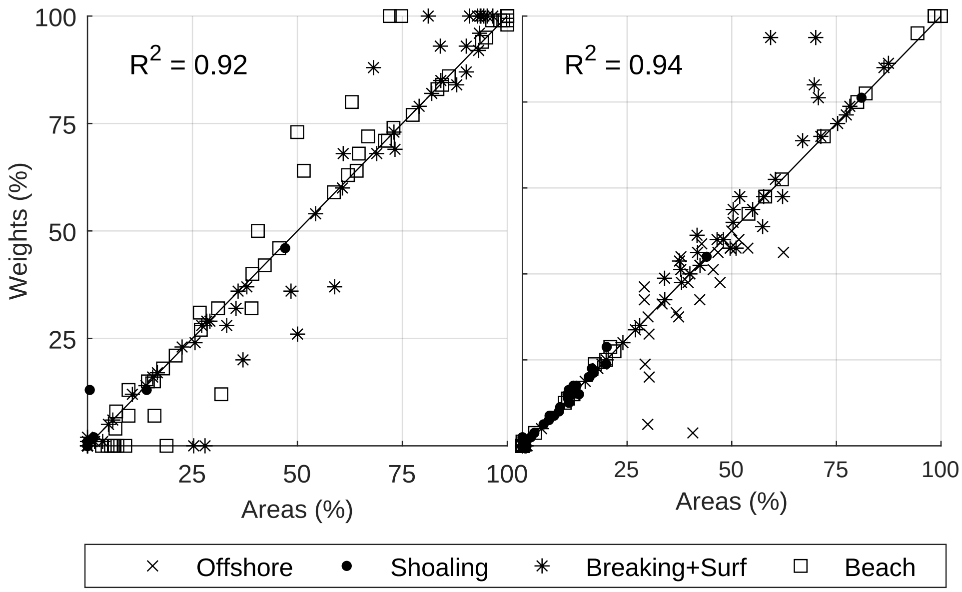

Figure 6: Scatter plots of concentrations of plastic debris collected and weighed in the laboratory (% of weights) and from image processing (% of areas) for initial plastic distributions in the run-up zone (IC_{shore}, left panel) and initial distributions along the wave flume ($IC_{dsitributed}$, right panel).

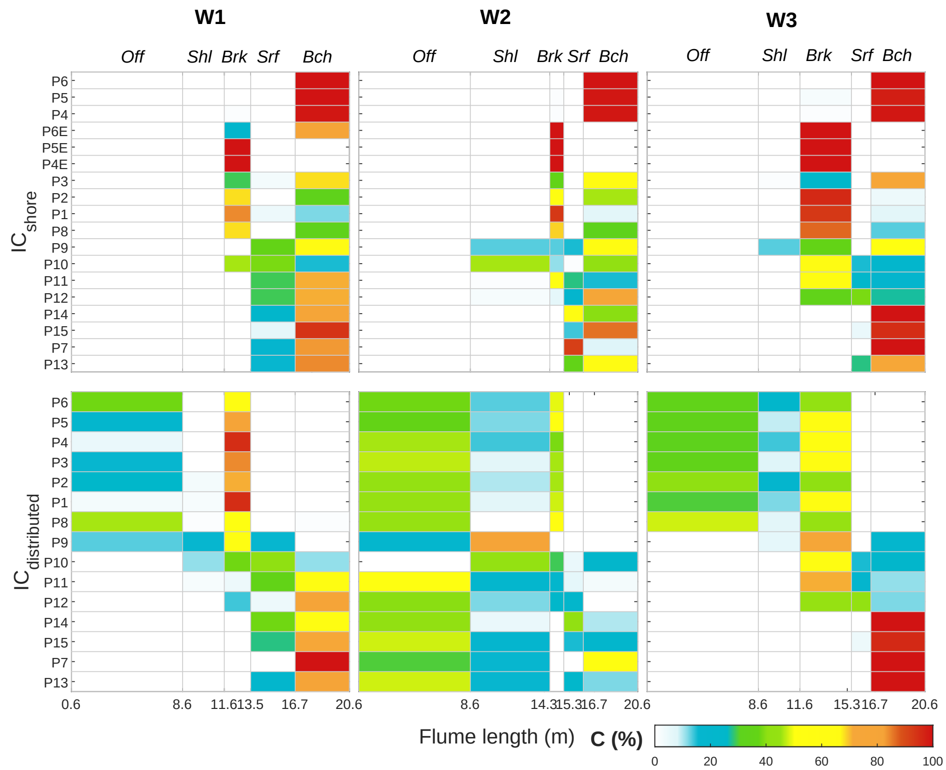

Figure 7: Cross-shore distribution of plastic debris under W1, W2, and W3 wave conditions for IC_{shore} (upper panels) and d$IC_{distributed}$ (lower panels). Note that the extension of each area (i.e., width of the columns) varies as a function of the position of the wave breaking.

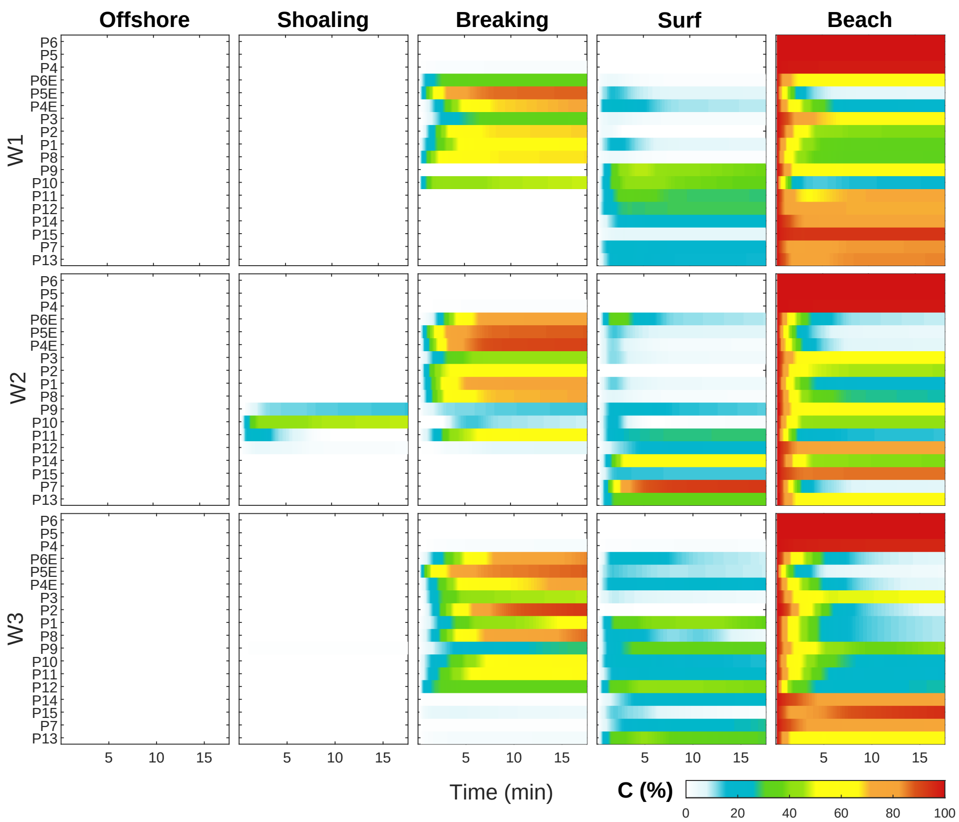

Figure 8: Temporal evolution of plastic-debris concentrations (C) for IC_{shore}.

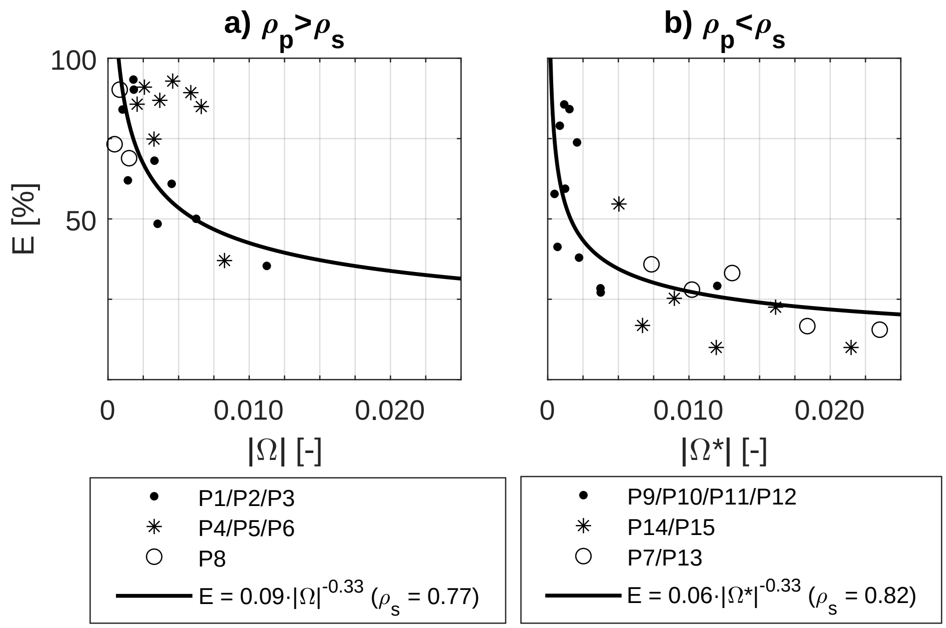

Figure 9: Relationship between the escape rates (E) of plastic debris and the dimensionless parameters Ω and Ω^* for plastic debris with a density greater (left panel) and less (right panel) than that of the water, respectively.

	ω_s^* –	β %		ω_r^* –	β %
***P*6**[1]	–	100.0	***P*9**	0.28	40.6
***P*5**[1]	–	100.0	***P*10**	0.22	21.0
***P*4**[1]	–	96.4	***P*11**	0.48	18.0
P6E	1.24	7.0	***P*12**	0.55	27.0
P5E	1.13	3.4	***P*14**	2.11	74.7
P4E	1.42	6.4	***P*15**	2.15	95.0
***P*3**	0.90	50.0	***P*7**	1.90	72.0
***P*2**	1.52	6.6	***P*13**	2.61	67.0
***P*1**	1.94	9.8			
***P*8**	3.68	9.8			

Table 2: *Beaching* (β) (%) from laboratory experiments under the irregular wave condition W3. [1]*Elongated plastic debris with a high degree of packing on land constitutes a new elemental unit whose* ω_s *was not inferred.*

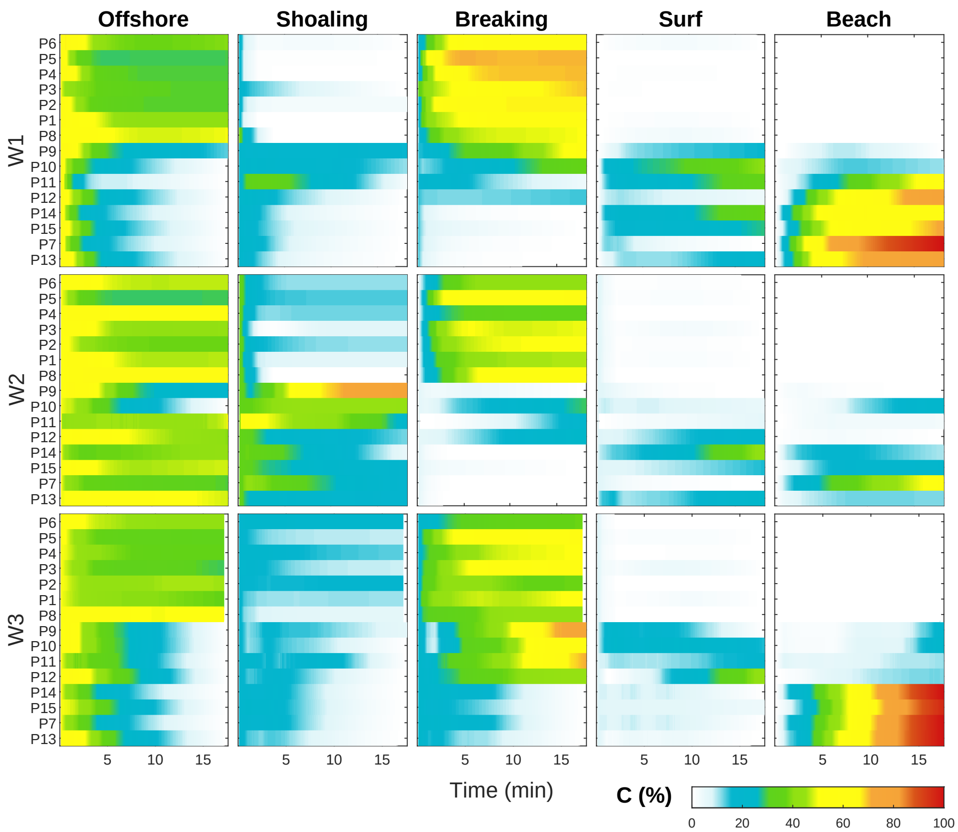

Figure 10: Temporal evolution of plastic-debris concentrations (C) for $IC_{distributed}$.

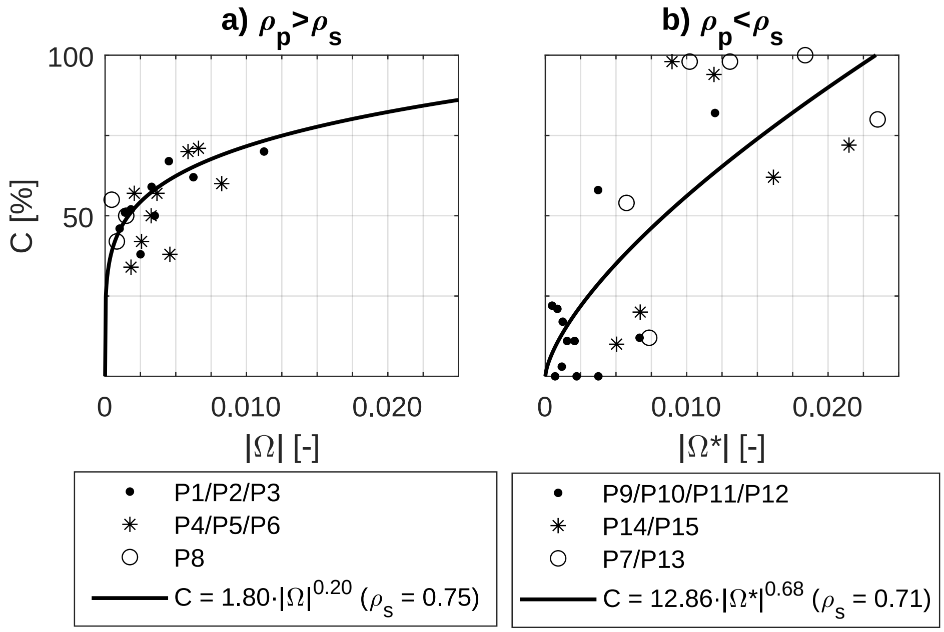

Figure 11: Relationship between the concentrations (C) of plastic debris on the breaking (left panel) and beach zones (right panel) and the dimensionless parameters Ω and Ω^* for plastic debris with a density greater (left panel) and less (right panel) than that of the water, respectively.